Chemistry–A European Journal

Full Paper
doi.org/10.1002/chem.202001739

Chemistry
Europe
European Chemical
Societies Publishing

▋ Radicals

A Mechanistic Study on Reactions of Group 13 Diyls LM with Cp*SbX₂: From Stibanyl Radicals to Antimony Hydrides

Christoph Helling,[a] Christoph Wölper,[a] George E. Cutsail III,[b] Gebhard Haberhauer,[c] and Stephan Schulz*[a]

Abstract: Oxidative addition of Cp*SbX₂ (X=Cl, Br, I; Cp*=C₅Me₅) to group 13 diyls LM (M=Al, Ga, In; L=HC[C(Me)N(Dip)]₂, Dip=2,6-iPr₂C₆H₃) yields elemental antimony (M=Al) or the corresponding stibanylgallanes [L(X)Ga]Sb(X)Cp* (X=Br **1**, I **2**) and -indanes [L(X)In]Sb(X)Cp* (X=Cl **5**, Br **6**, I **7**). **1** and **2** react with a second equivalent of LGa to eliminate decamethyl-1,1′-dihydrofulvalene (Cp*₂) and form stibanyl radicals [L(X)Ga]₂Sb˙ (X=Br **3**, I **4**), whereas analogous reactions of **5** and **6** with LIn selectively yield stibanes [L(X)In]₂SbH (X=Cl **8**, Br **9**) by elimination of 1,2,3,4-tetramethylfulvene. The reactions are proposed to proceed via formation of [L(X)M]₂SbCp* as reaction intermediate, which is supported by the isolation of [L(Cl)Ga]₂SbCp (**11**, Cp=C₅H₅). The reaction mechanism was further studied by computa-

tional calculations using two different models. The energy values for the Ga- and the In-substituted model systems showing methyl groups instead of the very bulky Dip units are very similar, and in both cases the same products are expected. Homolytic Sb–C bond cleavage yields van der Waals complexes from the as-formed radicals ([L(Cl)M]₂Sb˙ and Cp*˙), which can be stabilized by hydrogen atom abstraction to give the corresponding hydrides, whereas the direct formation of Sb hydrides starting from [L(Cl)M]₂SbCp* via concerted β-H elimination is unlikely. The consideration of the bulky Dip units reveals that the amount of the steric overload in the intermediate **I** determines the product formation (radical vs. hydride).

Introduction

Monovalent group 13 metal compounds of the general type RM (R=Cp*, L, others; Cp*=C₅Me₅, L=HC[C(Me)N(Dip)]₂) have been extensively studied over the last decade due to their interesting structures and unusual chemical reactivity.[1] These compounds not only serve as powerful two-electron reduction reagents, but also as potential Lewis bases or Lewis acids due to the presence of an electron lone pair as well as an empty p-

orbital, respectively. This unusual electronic nature with some similarities to group 14 carbenes lead to a unique chemical reactivity.

Cp*- and β-diketiminate-substituted derivatives for example were successfully applied as σ-donor ligands in transition metal chemistry,[2] Lewis acid-base reactions with main group metal compounds,[3] and bond activation reactions of a large variety of organic compounds.[4] Their reactivity in oxidative addition reactions originates from the M-centered (M=Al, Ga, In) electron lone pair (HOMO) as well as from the formally vacant p-orbital (LUMO+1), which makes these monovalent species particularly useful as strong nucleophiles and moderate electrophiles. According to quantum chemical calculations, the singlet-triplet energy gap (Al 46 kcal mol⁻¹; Ga 54 kcal mol⁻¹; In 55 kcal mol⁻¹) and HOMO–LUMO+1 separation (Al 82.8 kcal mol⁻¹; Ga 95.3 kcal mol⁻¹; In 95.9 kcal mol⁻¹) increase from Al to Ga, whereas those of Ga and In are virtually identical.[5] A monomeric alanediyl LAl[6] containing a sterically demanding N,N′-chelating β-diketiminate ligand was found to activate a large variety of main group element-hydrogen σ-bonds (H–X; X=H, B, C, Si, N, P, O)[7] as well as C–F and C–O σ-bonds,[8] whereas the corresponding gallanediyl LGa[9] shows a remarkable activity toward insertion reactions into main group metal-X bonds of heavy group 13 (Ga, In),[10] 14 (Ge, Sn, Pb),[11] 15 (Bi),[12] and 16 elements (Te).[13] In contrast, LIn is less reactive due to the enhanced stability of In in the +I oxidation state.[14]

Very recently, we started to investigate bond activation reactions of group 15 element compounds with group 13 diyls.[15]

[a] C. Helling, Dr. C. Wölper, Prof. Dr. S. Schulz
Institute for Inorganic Chemistry and
Center for Nanointegration Duisburg-Essen (Cenide)
University of Duisburg-Essen
Universitätsstraße 5–7, 45117 Essen (Germany)
E-mail: stephan.schulz@uni-due.de

[b] Dr. G. E. Cutsail III
Max Planck Institute for Chemical Energy Conversion (CEC)
Stiftstrasse 34–36/ 45470 Mülheim an der Ruhr (Germany)

[c] Prof. Dr. G. Haberhauer
Institute of Organic Chemistry
University of Duisburg-Essen
Universitätsstraße 5–7, 45117 Essen (Germany)

Chemistry–A European Journal

Full Paper
doi.org/10.1002/chem.202001739

Chemistry Europe
European Chemical
Societies Publishing

Reactions of EX$_3$ (E=As, Sb, Bi; X=halide, amide, alkoxide) with gallanediyl LGa typically occur with the insertion of LGa into the E−X bond (oxidative addition) followed by the elimination of LGaX$_2$. The outcome led to a variety of compounds with unusual bonding properties, that is, Ga-substituted dipnictenes [L(X)Ga]$_2$E$_2$ (E=As, Sb, Bi; X=halide, amide, alkoxide) with E=E double bonds,[16] tetrastiba- and tetrabismabicyclo[1.1.0]butane analogues [L(X)Ga]$_2$E$_4$ (E=Sb, Bi; X=Cl, NMe$_2$) with a central E$_4$ core,[17] as well as gallapnictenes [L(X)Ga]EGaL (E=As, Sb; X=halide) with Ga=E double bonds.[18] Based on the isolation of several carbene-stabilized stibinidenes ^{Me}CAAC-Sb[Ga(X)L] (^{Me}CAAC=cyclic (alkyl)(amino)carbene) and IDipp-Sb[Ga(X)L] (IDipp=1,3-bis(2,6-diisopropylphenyl)-imidazol-2-ylidene), the reactions were confirmed to proceed with the intermediate formation of Ga-substituted pnictinidenes [L(X)Ga]E.[19] In addition, reactions of LGa with [Cp*Sb]$_4$ yielded (LGa)$_2$Sb$_4$,[15c] whereas those with Cp*SbCl$_2$ and Cp*BiI$_2$ produced Sb- and Bi-centered radicals [L(Cl)Ga]$_2$Sb$^•$ (**A**) and [L(I)Ga]$_2$Bi$^•$ (**B**) (Scheme 1),[20] respectively. The formation of radicals A and B is accompanied by liberation of a centered Cp*$^•$ radical through a sterically induced homolytic E−C bond breakage of the precursor. [L(Cl)Ga]$_2$Sb$^•$ and [L(I)Ga]$_2$Bi$^•$ are both rare examples of neutral pnictogen-centered radicals, which are stable in solution and in the solid state.[21]

Recently, the same synthetic approach was extended to heteroleptic Sb-centered radicals of the type [{L(Cl)Ga}(R)]Sb$^•$ (**C**) (R=B[N(Dip)CH]$_2$, 2,6-Mes$_2$C$_6$H$_3$, N(SiMe$_3$)Dip; Mes=2,4,6-Me$_3$C$_6$H$_2$) (Scheme 1).[22] The influence of the ligand R on the electronic properties of the resulting radicals was thoroughly investigated. A strong dependence on the steric demand of the cyclopentadienyl substituent and the E−C bond strength was first observed in reactions of LGa with Cp*AsCl$_2$, which gave the gallaarsene LGa=AsCp* with a Ga=As double bond while retaining the As−C bond.[23] In contrast, the analogous reaction with Cp^{Ar}AsCl$_2$ (Cp^{Ar}=C$_5$(4-tBuC$_6$H$_4$)$_5$) containing the bulkier Cp^{Ar} ligand proceeded with As−C bond rupture to form the As-centered radical [L(Cl)Ga]$_2$As$^•$ (**D**) and the stable Cp$^{Ar•}$ radical.[24]

To determine the general applicability of this synthetic approach for group 15-centered radicals, we investigated the influence of the halide substituents in Cp*SbX$_2$ (X=F, Cl, Br, I), as well as the influence of the group 13 diyl LM (M=Al, Ga, In)
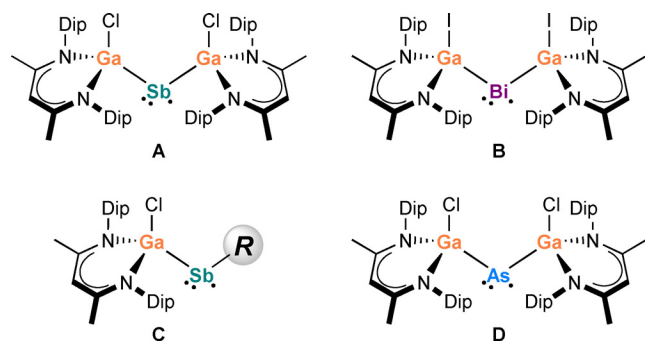
on the formation of antimony-centered radicals. In order to gain a deeper understanding of the reaction mechanism, the reactions of Cp*SbX$_2$ with LM were performed stepwise with different amounts of LM, which was furthermore studied by replacing the Cp* ligand in Cp*SbCl$_2$ with the less sterically demanding Cp ligand. In addition, computational calculations on the reaction mechanism were performed.
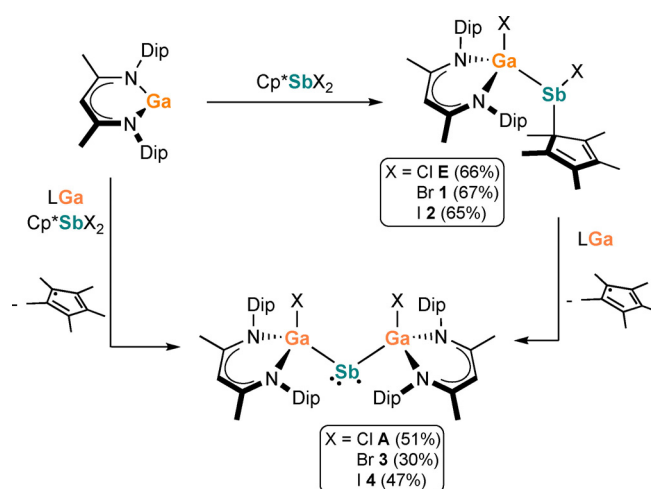
Results and Discussion

The influence of different cyclopentadienyl substituents on the reaction mechanism was already shown in reactions with Cp*EX$_2$ (E=As, Sb, Bi) and Cp^{Ar}AsCl$_2$.[20,23,24] To further study the effect of the halide substituent X in Cp*SbX$_2$ on the product formation and the role of the group 13 metal M in LM, we systematically studied reactions of three different group 13 diyls LM (M=Al, Ga, In) with four Cp*SbX$_2$ derivatives (X=F, Cl, Br, I).

Variation of the halide substituent X in Cp*SbX$_2$

Cp*SbF$_2$[25] and Cp*SbCl$_2$[25,26] were synthesized according to literature methods. Cp*SbBr$_2$ was reported to be formed in the reaction of Cp*Br with Sb powder.[27] However, both Cp*SbBr$_2$ and hitherto unknown Cp*SbI$_2$ were synthesized via more convenient salt metathesis reactions of KCp* with SbX$_3$. Cp*SbI$_2$ was structurally characterized by single-crystal X-ray diffraction (Figure S50 in Supporting Information). Cp*SbX$_2$ (X=F, Br, I) were then reacted with one equivalent of LGa. For Cp*SbF$_2$, an immediate reduction was observed under various conditions with formation of LGaF$_2$.[28] In contrast, reactions of Cp*SbCl$_2$, Cp*SbBr$_2$, and Cp*SbI$_2$ yielded [L(X)Ga]Sb(X)Cp* (X=Cl **E**,[20] Br **1**, I **2**). **1** and **2** were isolated as orange crystals suitable for X-ray diffraction (Scheme 2).

1 and **2** were further reacted with one equivalent of LGa, yielding stibanyl radicals [L(Br)Ga]$_2$Sb$^•$ (**3**) and [L(I)Ga]$_2$Sb$^•$ (**4**) in good yields. The observation of decamethyl-1,1′-dihydrofulvalene in the ^{1}H NMR spectrum strongly indicates the initial liber-

Scheme 1. Homo- and heteroleptic Gallium-substituted heavy group 15 element-centered radicals formed upon homolytic Sb−C bond breakage.

Scheme 2. Reactions of LGa with Cp*SbX$_2$. Yields in parentheses.

Chemistry–A European Journal

Full Paper
doi.org/10.1002/chem.202001739

**Chemistry
Europe**
European Chemical
Societies Publishing

ation of a Cp* radical during formation of **3** and **4**, which subsequently dimerized. **3** and **4** were also directly formed in reactions of Cp*SbX$_2$ (X = Br, I) with two equivalents of LGa, whereas the same reaction with Cp*SbF$_2$ only yielded LGaF$_2$[28] with no radical species observed even at low temperatures (−80 °C). Remarkably, reactions with Cp*SbBr$_2$ and Cp*SbI$_2$ are complete within 24 h, whereas that of Cp*SbCl$_2$ takes about seven days for completion.[20] These findings highlight the decreasing Sb−X bond strength with increasing atomic number of the halogen atom X. **3** and **4** were isolated in moderate yields as red crystals from deep red solutions upon storage at −30 °C (Scheme 1). In contrast to **A** and **3**, crystals of radical **4** are accessible from benzene and toluene solutions. They can be easily separated from minor side products such as LGaX$_2$, distibene [L(X)Ga]$_2$Sb$_2$, and gallastibene [L(X)Ga]SbGaL, which are formed in about 10% yield each as estimated by in situ ^{1}H NMR spectroscopy.

Compounds **1** and **2** are stable in the solid state at ambient temperature under argon atmosphere, but slowly decompose in solution to give LGaX$_2$ and Cp*$_2$ as was confirmed by ^{1}H NMR spectroscopy, as well as elemental antimony as was proven by EDX analysis. The respective ^{1}H and ^{13}C NMR spectra illustrate the asymmetric substitution at the Sb center, showing eight doublets and four septets that correspond to the CH*Me*$_2$ and CH*Me*$_2$ protons of the Dip groups, respectively. The C$_5$*Me*$_5$ protons appear as a single resonance at room temperature, indicative of fast sigmatropic shifts. The molecular structures of **1** (Figure 1) and **2** (Figure S43), which were determined by single-crystal X-ray diffraction,[29] show Ga−Sb bond lengths of 2.7058(5) Å (**1**) and 2.6567(5) Å (**2**), comparable to that of **E** (2.6979(2) Å). The Cp* ligands are coordinated to the Sb center in a κ^1 fashion with Sb−C bond lengths of 2.2441(16) Å (**1**) and 2.243(4) Å (**2**).

Radicals **3** and **4** are stable in the solid state and in solution at ambient temperature under argon atmosphere, but immediately decompose upon exposure to air and moisture. As is typ-
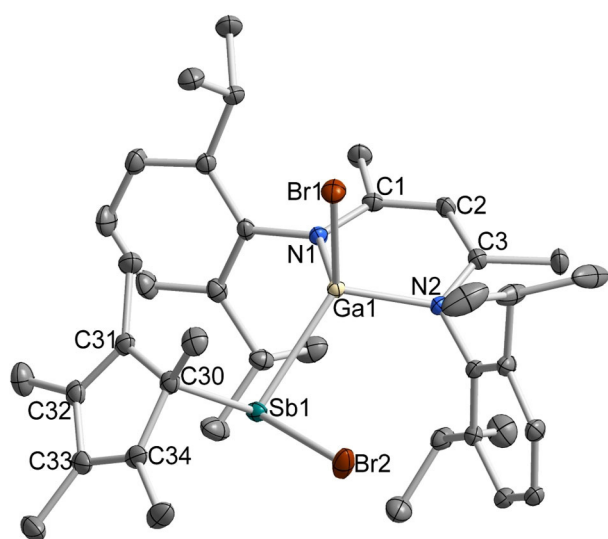
ical for paramagnetic species, their ^{1}H NMR spectra exhibit only broad resonances between −0.5 and 8 ppm. Based on the Evans method,[30] effective magnetic moments μ_{eff} of 1.62 μ_B (**3**) and 1.64 μ_B (**4**) were determined, which confirm a paramagnetic character due to the presence of a single unpaired electron ($S = \frac{1}{2}$). A variable-temperature (VT) ^{1}H NMR study showed no signs of dimerization upon cooling solutions of **3** and **4** down to −80 °C. IR spectra do not reveal any absorption bands in the expected region for Sb−H moieties (1750–1900 cm^{-1}).[20] The electronic structures of **3** and **4** were also examined by EPR spectroscopy; the X-band EPR spectra of **3** and **4** are displayed in Figure 2 alongside with that of **A**.[20] The complicated, yet well resolved super-hyperfine pattern of the spectra is consistent with >80% spin population at the Sb center with significant unpaired spin distributed to the Ga ligands (≈8% to each).[20] No significant differences between the EPR spectra are observed. The high-field region of the EPR spectra offers a limited selection of transitions, allowing a thorough comparison where no differences in the g_3, A_3(Sb) or A_3(Ga)-values of **A**, **3**, and **4** can be distinguished. No resolved ^{35,37}Cl hyperfine was observed for the Cl atom in **A**.[20] Despite the larger hyperfine coupling constants of ^{79,81}Br and ^{121}I in comparison to Cl (>5x),[31] no further hyperfine splittings are observed, indicating minimal unpaired spin on the halides. The EPR parameters of Sb-centered radicals are very sensitive to the complexes' electronic structure, which may be influenced by geometry and secondary factors such as steric demand. The remarkable similarities between the EPR spectra of **A**, **3**, and **4** indicate that they have nearly identical local Sb p-orbital radical character and electronic structures. Therefore, the halide has minimal, if any direct influence on the electronics of the Sb radical center.
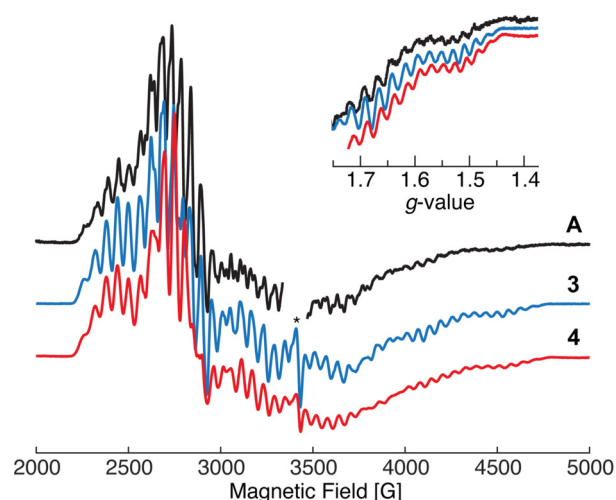
Figure 2. X-band (≈9.63 GHz) EPR spectra of **A**, **3**, and **4** in frozen toluene collected at 15 K. The asterisk at g ≈ 2 indicates a <1% organic radical impurity. The inset is an expansion of the high-field region on g-scale, correcting for slight shifts due to differences in microwave frequencies (±0.005 GHz). Spectrometer conditions: 100 kHz modulation frequency, 6 G modulation amplitude, 81.92 ms conversion time, 81.92 ms time constant, 4096 points. The spectrum of **A** is a replication of a previously published measurement collected under the same conditions, except for a 20.48 ms time constant.[20]

Figure 1. Molecular structure of **1**. Hydrogen atoms were omitted for clarity. Displacement ellipsoids are drawn at 50% probability level.

The molecular structures of **3** (Figure S44) and **4** (Figure 3) were determined by single-crystal X-ray diffraction. **3** and **4** show two-coordinated Sb centers, which adopt a bent geometry with Ga-Sb-Ga angles of 107.026(15)° (**3**) and 107.314(17)° (**4**) as summarized in Table 1. Due to the larger atomic radii of Br and I compared to Cl, these values are slightly larger compared to the Ga-Sb-Ga angle of **A** (104.890(10)°).[20] This trend is also reflected by the increasing Ga–X bond lengths (**A** 2.2028(7) Å, 2.1623(9) Å; **3** 2.3554(6) Å, 2.3556(6) Å; **4** 2.5789(5) Å, 2.5745(5) Å). In addition, the X1-Ga1···Ga2-X2 tor-
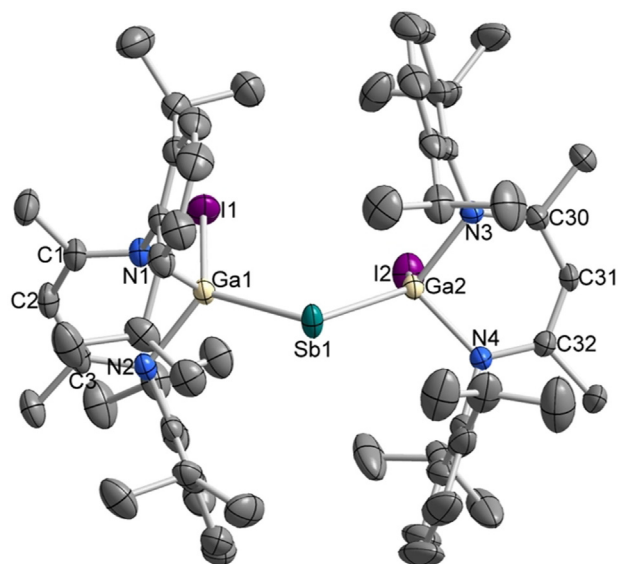
sion angles (**A** 41.36(3)°, **3** 34.52(2)°, **4** 32.75(2)°)[20] steadily decrease with increasing atomic number of the halide. The Sb–Ga bond lengths observed for radicals **A** (2.5899(4) Å, 2.5909(3) Å), **3** (2.5930(5) Å, 2.5849(4) Å), and **4** (2.5833(5) Å, 2.5936(5) Å) are virtually identical and agree with the values observed for similar Sb compounds containing [L(X)Ga] ligands.[16–19,22]
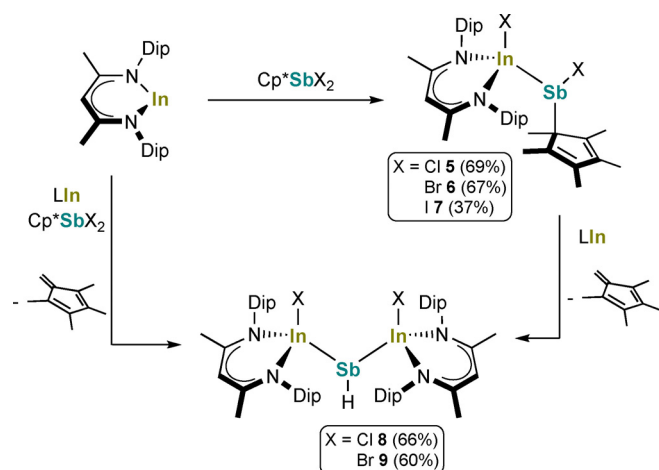
Variation of group 13 metal M in LM

The specific role of the group 13 metal center in LM (M = Al, Ga, In) was studied to evaluate the general applicability of this approach. Reactions of LAl with Cp*SbX$_2$ (X = F, Cl, Br, I) in different stoichiometries (1:1 to 1:3), solvents and at various reaction temperatures all led to a complete reduction of Cp*SbX$_2$ with formation of Sb metal (EDX analysis) and LAlX$_2$. This outcome coincides with the strong reducing properties of LAl, which was expected to be the strongest reductant among the tested group 13 diyls. On the other hand, equimolar reactions of LIn with Cp*SbX$_2$ (Scheme 3) led to clean formation of insertion products [L(X)In]Sb(X)Cp* (X = Cl **5**, Br **6**, I **7**), except for Cp*SbF$_2$ which yielded intractable mixtures of products, from which no insertion compound could be isolated.

Upon workup, compounds **5**–**7** were isolated as orange crystals in moderate yields. Their ^{1}H and ^{13}C NMR spectra are comparable to those of the Ga-analogues **E**, **1** and **2** (see above), showing eight doublets and four septets for the CH*Me*$_2$ and CH*Me*$_2$ protons as well as single resonances for the C$_5$*Me*$_5$ protons. As was observed for **1** and **2**, compounds **5**–**7** are stable in the solid state, but slowly decompose in solution at ambient temperature.

Figure 3. Molecular structure of **4**. Hydrogen atoms were omitted for clarity. Displacement ellipsoids are drawn at 50 % probability level.

Table 1. Central bond lengths [Å] and angles [°] of [L(X)Ga]Sb(X)Cp* (**E**, **1**, **2**), [L(X)In]Sb(X)Cp* (**5**–**7**), [L(X)Ga]$_2$Sb$^•$ (**A**, **3**, **4**), and [L(X)In]$_2$SbH (**8**, **9**); X = Cl, Br, I.

| | [L(X)Ga]Sb(X)Cp* | | | | [L(X)In]Sb(X)Cp* | | |
	E[a]	**1**	**2**		**5**	**6**	**7**
Ga—Sb	2.6979(2)	2.7058(5)	2.6567(5)	In—Sb	2.8317(3)	2.8333(3)	2.8340(2)
Ga—N	1.9571(13)	1.9573(13)	1.9592(15)[b]	In—N	2.1530(10)	2.1546(10)	2.1654(13)
	1.9719(13)	1.9783(13)			2.1708(10)	2.1747(10)	2.1862(13)
Sb—C	2.2381(16)	2.2441(16)	2.243(4)	Sb—C	2.2325(12)	2.2365(12)	2.2429(16)
Ga—Sb-C	106.83(4)	107.60(4)	110.72(9)	In-Sb-C	102.58(3)	103.16(3)	104.50(4)
Ga-Sb-X	93.614(13)	94.094(7)	98.216(12)	In-Sb-X	90.580(9)	90.594(5)	91.293(5)
N-Ga-N	95.47(5)	95.53(5)	96.56(9)	N-In-N	89.09(4)	89.24(4)	89.80(5)
X-Sb-C	94.68(5)	94.84(4)	98.51(10)	X-Sb-C	97.08(3)	97.09(3)	96.73(4)

| | [L(X)Ga]$_2$Sb$^•$ | | | | [L(X)In]$_2$SbH | |
	A[a]	**3**	**4**		**8**	**9**
Ga—Sb	2.5899(4)	2.5849(4)	2.5833(5)	In—Sb	2.7348(5), 2.7384(5)	2.7250(4), 2.7347(3)
	2.5909(3)	2.5930(5)	2.5936(5)		2.7382(5), 2.7472(5)	
Ga—N	1.9558(19), 1.9594(19)	1.956(3), 1.965(3)	1.964(3), 1.985(3)	In—N	2.143(3), 2.151(3)	2.144(3), 2.157(3)
	1.9607(19), 1.9693(19)	1.952(3), 1.975(3)	1.965(3), 1.967(3)		2.150(3), 2.161(3)	2.147(3), 2.166(3)
					2.151(3), 2.154(3)	
					2.145(3), 2.151(3)	
Ga-Sb-Ga	104.890(10)	107.026(15)	107.314(17)	In-Sb-In	101.78(2), 100.94(2)	98.60(2)
N-Ga-N	95.78(8),	95.84(11),	96.09(13),	N-In-N	89.57(11), 90.21(12)	89.83(11), 89.97(12)
	95.69(8)	95.73(11)	95.58(12)		89.06(11), 90.14(11)	

[a] The syntheses and solid-state structures of **A** and **E** were reported previously; [b] Identical values due to special position.[18]

Chemistry–A European Journal

Full Paper
doi.org/10.1002/chem.202001739

**Chemistry
Europe**
European Chemical
Societies Publishing

Scheme 3. Reactions of LIn with Cp*SbX₂. Yields in parentheses.

The molecular structures of **5–7** (Figure 4, Figures S45, S46 in Supporting Information) reveal the presence of rare Sb–In bonds with virtually identical bond lengths of 2.8317(3) Å (**5**), 2.8333(3) Å (**6**), and 2.8340(2) Å (**7**), that are comparable to those reported for [R₂SbInR′₂]ₓ (2.824–2.934 Å; $x = 2, 3$; R = Me, SiMe₃; R′ = Me, Et, tBu, CH₂SiMe₃).[32] The Cp* ligands adopt a κ^1-coordination with Sb–C bond lengths of 2.2325(12) Å (**5**), 2.2365(12) Å (**6**), and 2.2429(16) Å (**7**).

Reactions of Cp*SbX₂ (X = Cl, Br) with two equivalents of LIn (Scheme 3), as well as treatment of either **5** or **6** with one equivalent of LIn at ambient temperature all produce orange solutions over the course of several hours. Crystallization from solutions in hexane yielded pale yellow crystals, which were identified as In-substituted antimony hydrides [L(X)In]₂SbH (X = Cl **8**, Br **9**). The reactions proceed without formation of significant amounts of side products as was proven by ¹H NMR spectroscopy. In contrast, no clean reactions were observed with Cp*SbF₂ and Cp*SbI₂ such that neither hydrides nor radical

species could be isolated. However, an in situ monitoring of Cp*SbI₂ with LIn by ¹H NMR spectroscopy revealed trace amounts of [L(I)In]₂SbH due to the appearance of a resonance at −2.56 ppm (Figure S31). A comparable resonance was not found in the reaction of LIn with Cp*SbF₂. The formation of **8** and **9** is astonishing as it raises the question about the origin of the Sb-bound hydrogen atom. The observation of the reaction progress by in situ ¹H NMR spectroscopy revealed a simultaneous production of 1,2,3,4-tetramethylfulvene, which was identified by its characteristic methylene proton resonance at 5.34 ppm.[33] Interestingly, a similar fulvene elimination/E-H (E = P, As) bond formation reaction was observed upon the phosphine coordination of Cp*-substituted bridged pentelidene complexes.[34]

¹H and ¹³C NMR spectra of compounds **8** and **9** show the expected resonances of the β-diketiminate ligand. The Sb−H resonances are found at higher field (**8** −3.42 ppm, **9** −3.07 ppm) compared to Dmp₂SbH (5.18 ppm) (Dmp = 2,6-Mes₂C₆H₃),[35] [O(Me₂SiNDip)₂]SbH (11.34 ppm)[36] and [L(Cl)Ga]Sb(H)Cp* (2.73 ppm).[20] A similar shift was only reported for [Me₃N(H)₂B]₂SbH (−2.48 ppm),[37] which contains two electropositive B-based substituents at Sb. The presence of the Sb−H moieties was further proven by IR spectroscopy, which featured characteristic bands at 1846 and 1848 cm⁻¹ for **8** and **9**, respectively. These values are in accordance to the reported values of antimony hydrides.[20,35–37] The molecular structures of **8** (Figure 5) and **9** (Figure S47) were determined by single-crystal X-ray diffraction.

Unfortunately, the Sb-bound hydrogen atoms could not be located on the electron density map, which could possibly be due to a two-fold disorder of the hydride ligand relative to the In-Sb-In plane. Nevertheless, its existence was unambiguously proven by ¹H NMR and IR spectroscopy. The Sb−In bond lengths of the two independent moieties of **8** (molecule 1: 2.7348(5) Å, 2.7384(59 Å; molecule 2: 2.7382(5) Å, 2.7472(5) Å) compare well to those of **9** (2.7250(4) Å, 2.7347(3) Å), but are
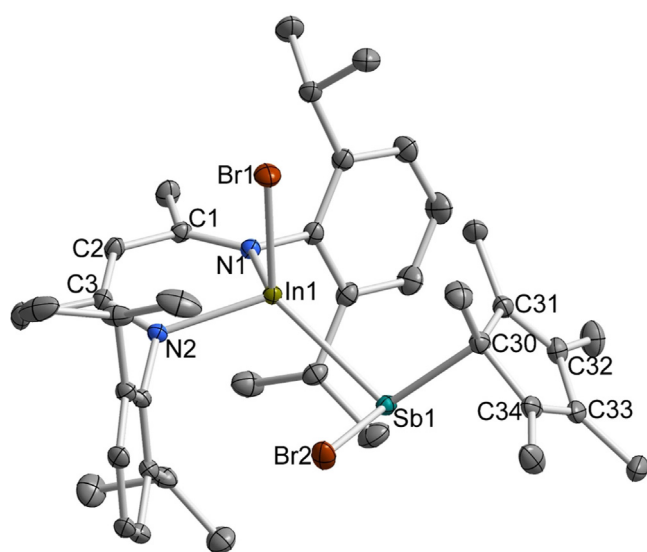

Figure 4. Molecular structure of **6**. Hydrogen atoms were omitted for clarity. Displacement ellipsoids are drawn at 50 % probability level.
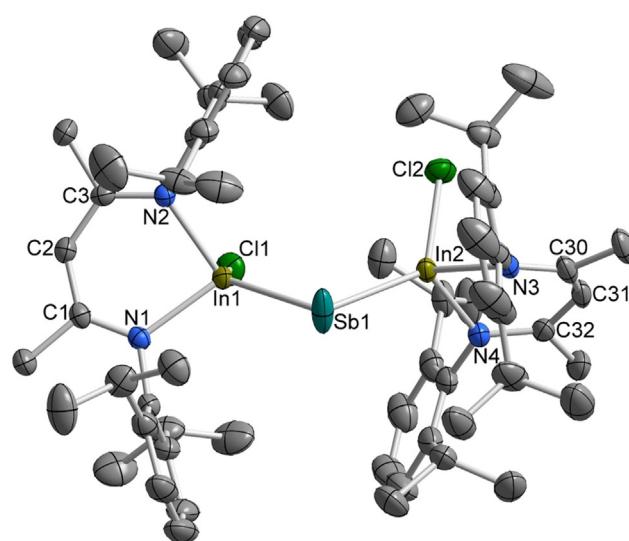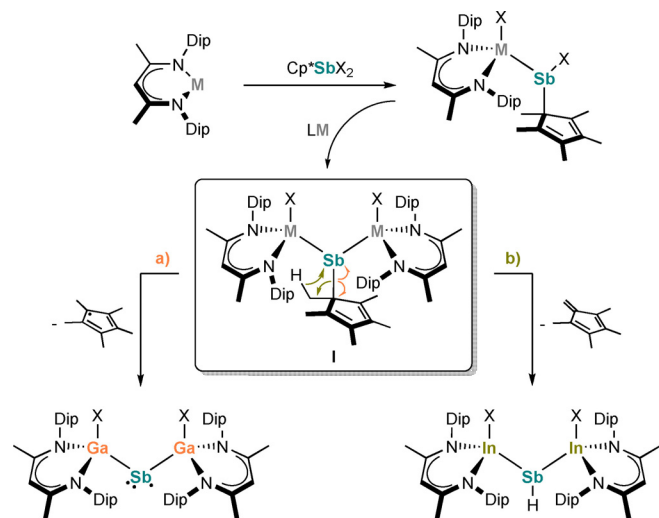

Figure 5. Molecular structure of **8**. Hydrogen atoms were omitted for clarity. Displacement ellipsoids are drawn at 50 % probability level.

Chemistry–A European Journal

Full Paper
doi.org/10.1002/chem.202001739

Chemistry Europe
European Chemical
Societies Publishing

considerably shorter than those of **5**–**7**. The same trend is observed for **A**, **3**, and **4** in comparison to **E**, **1**, and **2** (Table 1), which can be either explained by a stronger backdonation from the electron-rich Sb in the [L(X)M]$_2$Sb motives[22] or by enhanced dispersion forces between the Dip groups of the β-diketiminate ligands.[16c, 19] The In-Sb-In angles (**8** molecule 1: 101.775(15)°, molecule 2: 100.943(15)°; **9** 98.602(11)°) are comparable yet slightly sharper than those in **A**, **3**, and **4**, presumably due to the decreased steric bulk of the [L(X)In] ligands compared to [L(X)Ga] (see below).
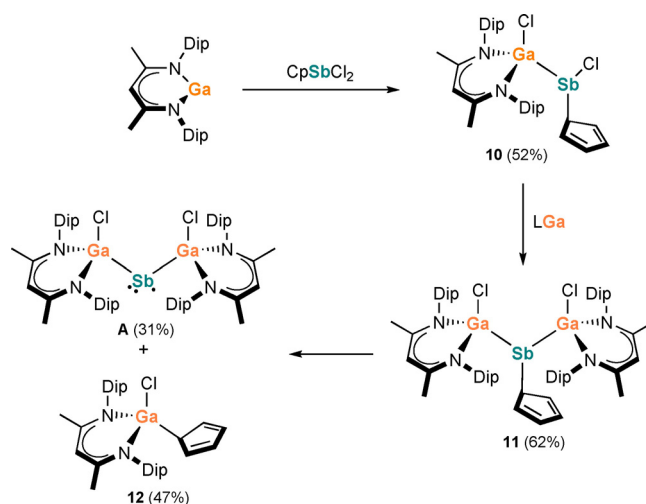
Investigation of the reaction mechanism

To provide an explanation for the observed radical (LGa) versus the hydride formation (LIn), the underlying reaction mechanism was studied in more detail. Similar to the analogous reactions of antimony trihalides SbX$_3$ with LGa,[19] we propose a mechanism that includes a sequential two-fold insertion of LM into the Sb–X bonds of Cp*SbX$_2$ which initially yields [L(X)M]Sb(X)Cp* (compounds **E**, **1**, **2**, **5**, **6**, **7**), followed by a short-lived intermediate of the type [L(X)M]$_2$SbCp* (**I**). Although such an intermediate could neither be isolated nor observed by in situ ^{1}H NMR spectroscopy, the high degree of steric congestion in **I** likely leads to the liberation of the most labile ligand in the system, namely η^1-Cp*. This step proceeds via two potential pathways: a) Sb–C bond homolysis with the formation of radical [L(X)Ga]$_2$Sb• and Cp*• or b) synchronous or asynchronous β-H elimination with the formation of hydride [L(X)In]$_2$SbH and 1,2,3,4-tetramethylfulvene (Scheme 4).

In order to detect proposed intermediates such as **I**, LM was reacted with CpSbCl$_2$, which contains the sterically less demanding Cp (Cp=C$_5$H$_5$) substituent. Reactions with one equivalent of LGa yielded [L(Cl)Ga]Sb(Cl)Cp (**10**), while reactions with two equivalents of LGa gave [L(Cl)Ga]$_2$SbCp (**11**) (Scheme 5). These results support the proposed reaction mechanism. Unfortunately, similar reactivities were not observed for

Scheme 5. Synthesis of **10** and **11** and decomposition of **11** yielding **A** and **12**. Yields in parentheses.

LAl and LIn, instead, dark insoluble materials were obtained with different solvents and reaction temperatures.

10 and **11** were isolated as colourless and yellow crystals, respectively, which are stable in the solid state, but decompose in solution (see below). The ^{1}H and ^{13}C NMR spectra of **10** show the expected resonances of the corresponding ligands (L, Cp) in a 1:1 ratio and appear overall very similar to those of insertion compounds **E**, **1**, **2**, **5**, **6**, and **7**. Compound **11** shows several broad resonances in the ^{1}H NMR spectrum at ambient temperature due to dynamic processes, which became sharper upon cooling to −60 °C. Two distinct signals of the γ-C*H* protons of both magnetically inequivalent β-diketiminate ligands and four resonances corresponding to the C$_5$H$_5$ protons were observed under these conditions (Figure S35). The solid-state structures of **10** (Figure S48) and **11** (Figure 6) feature κ^1-coor-

Scheme 4. Proposed reaction mechanism yielding either radicals [L(X)Ga]$_2$Sb• by route a) or hydrides [L(X)In]$_2$SbH by route b).
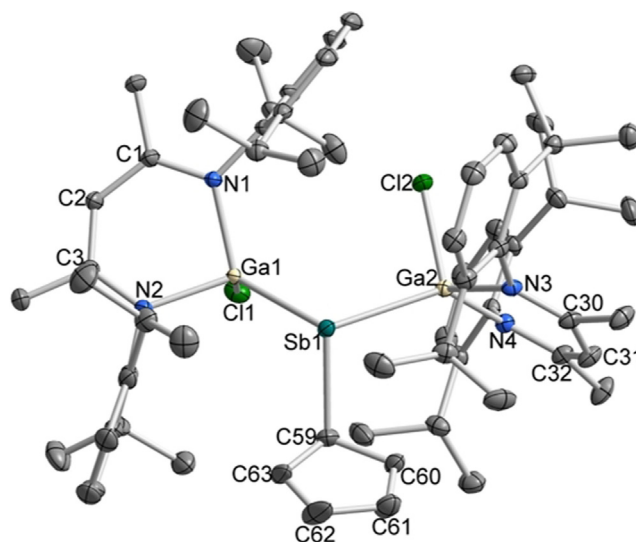

Figure 6. Molecular structure of **11**. Hydrogen atoms and two molecules of toluene were omitted for clarity. Displacement ellipsoids are drawn at 50% probability level.

Chemistry–A European Journal

Full Paper
doi.org/10.1002/chem.202001739

Chemistry Europe
European Chemical
Societies Publishing

dinated Cp ligands at Sb with Sb—C bond lengths of 2.221(3) Å (**10**) and 2.2396(12) Å (**11**), which are in good agreement with the Cp*-substituted complexes **E**, **1**, **2**, **5**, **6**, and **7**. The Ga—Sb bond lengths (**10** 2.6453(5) Å; **11** 2.6472(5) Å, 2.6352(5) Å) lie within the expected range,[16–19,22] while the Ga-Sb-Ga bond angle in **11** (106.838(13)°) is similar to those in radicals **3** and **4**,[20] but considerably wider than that in [L(Cl)Ga]₂SbDip (97.603(7)°).[24]

11 is unstable in solution and decomposes slowly at ambient temperature but much faster at elevated temperature (60 °C), yielding stibanyl radical **A** and LGa(Cl)Cp as side product (**12**) in moderate yields (Scheme 5, Figure S49). The formation of **A** shows the tendency of homolytic Sb—C cleavage of cyclopentadienyl-substituted stibanes and supports the proposed mechanism (Scheme 4). However, the formation of **12** shows that besides homolytic pathways, heterolytic/polar pathways are also accessible depending on the nature of the ligand.

Furthermore, the origin of the observed radical versus hydride selectivity was investigated by quantum chemical calculations. **13** and **14** were chosen as model systems with methyl groups instead of the very bulky Dip units (Scheme 6). These models allow to separate electronic influences from steric effects. In the first step, the two possible reaction pathways (homolysis under formation of radical and β-H elimination under formation of hydride) were calculated. In order to optimize the structures, the density functional method B3LYP[38] and additional dispersion correction with Becke–Johnson damping[39] (D3BJ) were used. As basis sets, 6-31G(d) was employed for the elements C, H, N, and Cl, whereas def2-TZVP was applied for Ga, In and Sb. Furthermore, single-point calculations on the optimized structures were performed using B3LYP-D3BJ with the basis sets 6–311G(d,p) (C, H, N, and Cl) and def2-TZVPPD (for Ga, In and Sb). To determine the solvent effect, the single-point calculations were conducted using the SMD variation of a polarizable continuum model with benzene as the chosen solvent ($\epsilon = 2.2706$). Considering the existence of diradical species along the reaction pathways, the structures were computed as open-shell singlets using the UB3LYP function. This procedure provides reliable geometries and energies for singlet-state diradicals of large systems with diradical character where high-level ab initio calculations are not feasible.[40]

In order to calculate the homolytic bond cleavage (pathway a) in Scheme 6), the distance between the antimony and the carbon atom was fixed at given values and all other parameters were optimized by means of B3LYP-D3BJ. The resulting data are depicted in Figure 7.

An enlargement of the distance d(Sb—C) leads to a curve showing a sharp energy increase in the first part followed by a flat area in the second part. The first part corresponds to the cleavage of the Sb—C bond, while the second part represents the van der Waals complexes (**15** and **16**) between the two radicals ([L(Cl)M]₂Sb• and Cp*•). These diradicals are minima and about 30 kcal mol⁻¹ higher in energy than the corresponding intermediates **13** and **14**. In the case of the β-H elimination (pathway b) in Scheme 6), a relaxed surface scan of the Sb—H bond length was applied, where the distance between the antimony and the hydrogen atom was held constant at certain values. The obtained curves (Figure 8, left) show that the energy values raise to over 65 kcal mol⁻¹ at a 1.75 Å Sb—H distance for **13** and **14**, which is slightly larger than an expected Sb—H hydride distance (1.7 Å). This shows that **13** and **14** fail to form the corresponding van der Waals complexes between the antimony hydride and 1,2,3,4-tetramethylfulvene (**17** and **18**). Here, the β-H elimination does not occur for **13** and **14**, hence an alternative pathway for the formation of the hydride must be considered. One possibility is a stepwise mechanism: the first step is the formation of the diradicals **15** and **16** (pathway a) in Scheme 6), while the second step is the hydrogen atom abstraction from the Cp*• radical by the antimony radical (pathway c) in Scheme 6). The computed energy profile for this reaction yielded a curve (right side of Figure 8) with a flat area for large Sb—H distances, a transition state at about 2.1 Å,
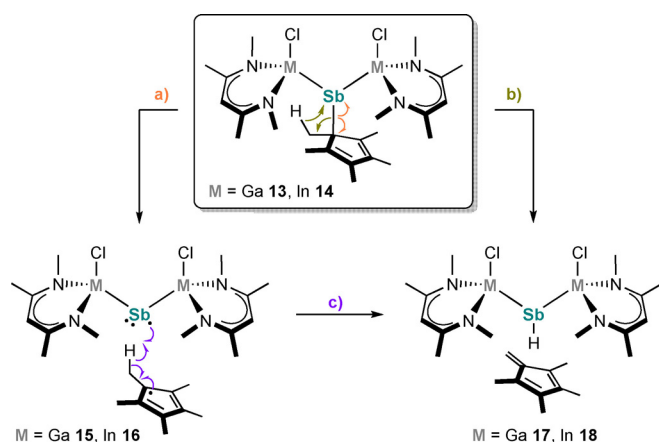
Scheme 6. Proposed reaction mechanism for the decay of intermediates **13** and **14** to the diradicals **15** and **16** as well as to the van der Waals complexes **17** and **18**.
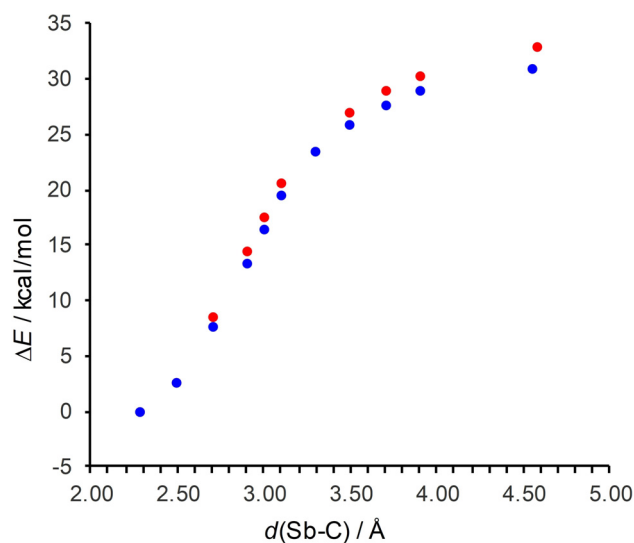
Figure 7. Energy profile for the Sb—C bond homolysis under formation of the van der Waals complex (**15** and **16**) between the two radicals [L(Cl)M]₂Sb• and Cp*• (blue: M=Ga; red: M=In).
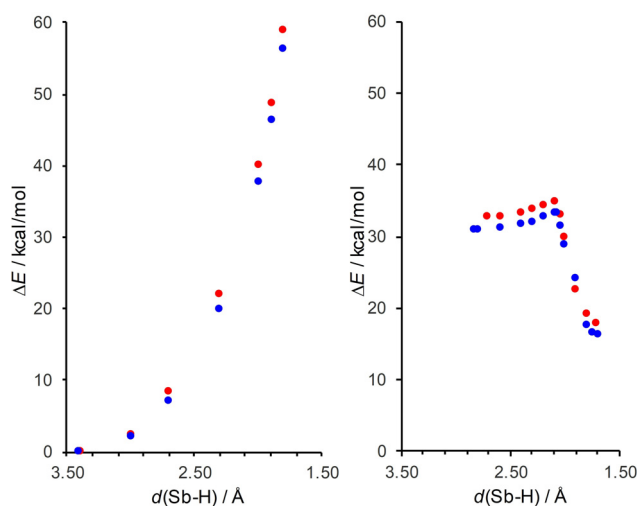
Chemistry–A European Journal

Full Paper
doi.org/10.1002/chem.202001739

Chemistry
Europe
European Chemical
Societies Publishing

Figure 8. Left: Energy profile for the decrease of the Sb—H bond in the intermediates **13** and **14** (blue: M = Ga; red: M = In). Right: Energy profile for the hydrogen atom abstraction from the Cp* radical by the antimony radical yielding the van der Waals complexes **17** and **18** (blue: M = Ga; red: M = In).

and a very steep part representing the formation of the Sb—H bond. The energy of the van der Waals complexes **17** and **18** is about 16 kcal mol^{-1} higher than that of the corresponding intermediates **13** and **14**.

The following conclusions can be drawn for the model systems **13** and **14**. The cleavage of the Sb—C bond is accompanied by high energetic effort. The diradicals can be stabilized by hydrogen atom abstraction yielding the corresponding hydrides, whereby the activation energy for this process is very low. The direct formation of the hydrides starting from the intermediates **13** and **14** via a concerted β-H elimination is unlikely. The energy values for the Ga- and the In-substituted systems are very similar, and in both cases the same products are expected.

A completely different picture emerges if the homolytic Sb—C bond cleavage (pathway a) and the subsequent hydrogen atom abstraction from the Cp* radical by the antimony radical (pathway c) are considered for the Dip-substituted systems (Figure 9). Due to the high steric overload in the Ga-substituted intermediate **Ia**, the radicals **A** and Cp* are more stable by ca. 11 kcal mol^{-1} than the intermediate **Ia**. For the subsequent hydrogen atom abstraction reaction, an activation energy of 19.2 kcal mol^{-1} is required. Hence, this abstraction does not occur, but a dimerization of the Cp* radical is observed. Consequently, radical **A** remains in solution. In the case of the In-substituted intermediate **Ib**, the radicals **F** and Cp* are less stable than **Ib** and the subsequent hydrogen atom abstraction, with an activation energy of about 10 kcal mol^{-1}, can occur, leading to the hydride **8** and 1,2,3,4-tetramethylfulvene. These findings lead to the following conclusion: the driving force for the Sb—C bond homolysis is the steric overload in the intermediate **I**. The higher the steric overload at the antimony atom, the higher the activation barrier for the subsequent hydrogen atom abstraction. In the case of the Ga-substituted system, the H-atom abstraction does not occur, hence only the radical is observed. The higher steric overload in the Ga-substituted intermediate **I** was assessed by comparing the buried volume calculations[41] of the [L(Cl)Ga] and [L(Cl)In] ligands. In the case of [L(Cl)Ga] (V_{bur} = 35.3%), the Sb center in [L(Cl)M]$_2$Sb$^•$ is by about 13% more encumbered in comparison to [L(Cl)In] (V_{bur} = 28.6%) (Figure S51).

Conclusions

A systematic study on reactions of Cp*SbX$_2$ with different amounts of LM were performed to gain a deep understanding on the reaction mechanism of these reactions and on the influence of the halide substituents as well as the group 13 metal. The reactions proceeded stepwise; first with the formation of

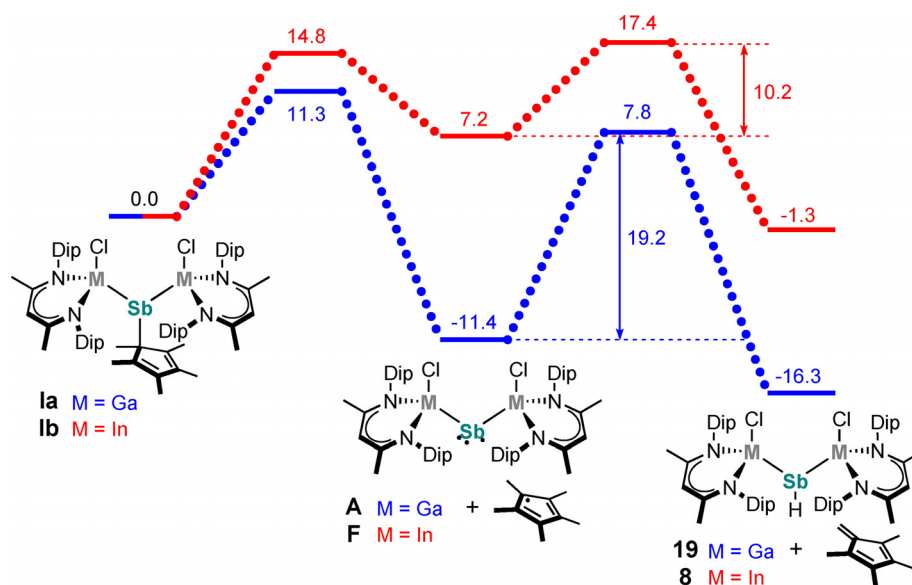**Figure 9.** Reaction of the intermediates **Ia-b** to the radicals [L(Cl)M]$_2$Sb$^•$ (**A** and **F**) and the hydrides [L(Cl)M]$_2$SbH (**8** and **19**) calculated by means of B3LYP-D3BJ. The indicated free-energies (ΔG) are given in kcal mol^{-1}.

Chemistry–A European Journal

| Full Paper
doi.org/10.1002/chem.202001739

Chemistry Europe
European Chemical
Societies Publishing

the corresponding mono-insertion products [L(X)M]Sb(X)Cp* (M = Ga, In; X = Cl, Br, I), followed by the formation of either Ga-substituted stibanyl radicals [L(X)Ga]$_2$Sb$^{\bullet}$ or In-substituted stibanes [L(X)In]$_2$SbH. The reactions with two equivalents of LM most likely proceed via formation of the double-insertion compounds [L(X)M]$_2$SbCp* as the reaction intermediate, which was supported by the synthesis of [L(Cl)Ga]$_2$SbCp, containing the sterically less demanding Cp substituent. Computational calculations gave more insights into the underlying reaction mechanism, suggesting that the formation of [L(X)In]$_2$SbH proceeds via a hydrogen atom abstraction from Cp*$^{\bullet}$ by intermediate [L(X)In]$_2$Sb$^{\bullet}$ radicals, rendering this process a stepwise β-H elimination that is mainly controlled by the steric environment.

Experimental Section

General Procedures: All manipulations were performed under an atmosphere of purified argon using standard Schlenk and glovebox techniques. Solvents were dried using a MBraun Solvent Purification System and were carefully degassed. Karl Fischer titration of the dry solvents show water levels less than 3 ppm. Deuterated NMR solvents were stored over activated molecular sieves (4 Å) and degassed prior to use. LAl,[6] LGa,[9] LIn,[14] Cp*SbX$_2$ (X = F,[26] Cl[26]) and CpSbCl$_2$[42] were prepared according to slightly modified literature procedures.

Instrumentation: ^{1}H (300, 500, 600 MHz) and ^{13}C{^{1}H} (75, 126, 151 MHz) NMR spectra (δ in ppm) were recorded using a Bruker Avance DPX-300, Bruker Avance DRX-500 or Bruker Avance III HD spectrometer and the spectra were referenced to internal [D$_6$]benzene (^{1}H: δ = 7.16; ^{13}C: δ = 128.06), [D$_8$]toluene (^{1}H: δ = 2.08; ^{13}C: δ = 20.43). Microanalyses were performed at the Elemental Analysis Laboratory of the University of Duisburg-Essen. IR spectra were measured in an ALPHA-T FTIR spectrometer equipped with a single reflection ATR sampling module, which is placed in a glovebox. Melting points were measured using a Thermo Scientific 9300 apparatus. Continuous-wave (CW) X-band ($\approx$9.63 GHz) EPR was collected on a Bruker E500 spectrometer equipped with an Oxford liquid helium flow cryostat and spectrometer conditions are detailed in the Figure caption.

Deposition Numbers 1994693 (**1**), 1994694 (**2**), 1994695(**3**), 1994697(**4**), 1994698 (**5**), 1994701 (**6**), 1994702 (**7**), 1994703 (**8**), 1994704 (**9**), 1994706 (**10**), 1994707 (**11**), 1994708 (**12**) and 1994709 (**Cp*SbI$_2$**) contain the supplementary crystallographic data for this paper. These data are provided free of charge by the joint Cambridge Crystallographic Data Center and Fachinformationszentrum Karlsruhe Access Structures service www.ccdc.cam.ac.uk/structures.

Full experimental details including spectroscopic (^{1}H, ^{13}C NMR, IR), crystallographic data and details of computational calculations are given in the Supporting Information.

Acknowledgements

Conflict of interest

The authors declare no conflict of interest.

[1] a) G. Linti, H. Schnöckel, *Coord. Chem. Rev.* **2000**, *206–207*, 285–319; b) M. N. Sudheendra Rao, H. W. Roesky, G. Anantharaman, *J. Organomet. Chem.* **2002**, *646*, 4–14; c) M. Asay, C. Jones, M. Driess, *Chem. Rev.* **2011**, *111*, 354–396; d) M. Zhong, S. Sinhababu, H. W. Roesky, *Dalton Trans.* **2020**, 1351–1364.

[2] a) S. González-Gallardo, T. Bollermann, R. A. Fischer, R. Murugavel, *Chem. Rev.* **2012**, *112*, 3136–3170; b) M. Molon, K. Dilchert, C. Gemel, R. W. Seidel, J. Schaumann, R. A. Fischer, *Inorg. Chem.* **2013**, *52*, 14275–14283; c) J. Weßing, C. Göbel, B. Weber, C. Gemel, R. A. Fischer, *Inorg. Chem.* **2017**, *56*, 3517–3525; d) C.-S. Cao, Y. Shi, H. Xu, B. Zhao, *Coord. Chem. Rev.* **2018**, *365*, 122–144.

[3] a) S. Schulz, A. Kuczkowski, D. Schuchmann, U. Flörke, M. Nieger, *Organometallics* **2006**, *25*, 5487–5491; b) M. Wiecko, P. W. Roesky, P. Nava, R. Ahlrichs, S. N. Konchenko, *Chem. Commun.* **2007**, 927–929; c) P. W. Roesky, *Dalton Trans.* **2009**, 1887–1893.

[4] a) T. Chu, G. I. Nikonov, *Chem. Rev.* **2018**, *118*, 3608–3680; b) Y. Liu, J. Li, X. Ma, Z. Yang, H. W. Roesky, *Coord. Chem. Rev.* **2018**, *374*, 387–415.

[5] C.-H. Chen, M.-L. Tsai, M.-D. Su, *Organometallics* **2006**, *25*, 2766–2773.

[6] C. Cui, H. W. Roesky, H.-G. Schmidt, M. Noltemeyer, H. Hao, F. Cimpoesu, *Angew. Chem. Int. Ed.* **2000**, *39*, 4274–4276; *Angew. Chem.* **2000**, *112*, 4444–4446.

[7] a) T. Chu, I. Korobkov, G. I. Nikonov, *J. Am. Chem. Soc.* **2014**, *136*, 9195–9202; b) T. Chu, S. F. Vyboishchikov, B. M. Gabidullin, G. I. Nikonov, *J. Am. Chem. Soc.* **2017**, *139*, 8804–8807.

[8] a) T. Chu, Y. Boyko, I. Korobkov, G. I. Nikonov, *Organometallics* **2015**, *34*, 5363–5365; b) M. R. Crimmin, M. J. Butler, A. J. P. White, *Chem. Commun.* **2015**, *51*, 15994–15996; c) L. Kong, R. Ganguly, Y. Li, R. Kinjo, *Chem. Eur. J.* **2016**, *22*, 1922–1925.

[9] N. J. Hardman, B. E. Eichler, P. P. Power, *Chem. Commun.* **2000**, 1991–1992.

[10] a) A. Kempter, C. Gemel, R. A. Fischer, *Inorg. Chem.* **2008**, *47*, 7279–7285; b) C. Ganesamoorthy, D. Bläser, C. Wölper, S. Schulz, *Organometallics* **2015**, *34*, 2991–2996.

[11] a) G. Prabusankar, A. Kempter, C. Gemel, M.-K. Schröter, R. A. Fischer, *Angew. Chem. Int. Ed.* **2008**, *47*, 7234–7237; *Angew. Chem.* **2008**, *120*, 7344–7347; b) G. Prabusankar, C. Gemel, M. Winter, R. W. Seidel, R. A. Fischer, *Chem. Eur. J.* **2010**, *16*, 6041–6047; c) A. Doddi, C. Gemel, M. Winter, R. A. Fischer, C. Goedecke, H. S. Rzepa, G. Frenking, *Angew. Chem. Int. Ed.* **2013**, *52*, 450–454; *Angew. Chem.* **2013**, *125*, 468–472.

[12] G. Prabusankar, C. Gemel, P. Parameswaran, C. Flener, G. Frenking, R. A. Fischer, *Angew. Chem. Int. Ed.* **2009**, *48*, 5526–5529; *Angew. Chem.* **2009**, *121*, 5634–5637.

[13] S. Schulz, C. Ganesamoorthy, G. Bendt, D. Bläser, C. Wölper, *Dalton Trans.* **2015**, *44*, 7048.

[14] M. S. Hill, P. B. Hitchcock, *Chem. Commun.* **2004**, 1818–1819.

[15] a) C. Ganesamoorthy, D. Bläser, C. Wölper, S. Schulz, *Chem. Commun.* **2014**, *50*, 12382–13284; b) C. Ganesamoorthy, D. Bläser, C. Wölper, S. Schulz, *Angew. Chem. Int. Ed.* **2014**, *53*, 11587–11591; *Angew. Chem.* **2014**, *126*, 11771–11775; c) C. Ganesamoorthy, J. Krüger, C. Wölper, A. S. Nizovtsev, S. Schulz, *Chem. Eur. J.* **2017**, *23*, 2461–2468; d) C. Ganesamoorthy, J. Krüger, C. Wölper, E. Glöckler, C. Helling, L. John, W. Frank, C. Wölper, S. Schulz, *Inorg. Chem.* **2018**, *57*, 9495–9503.

[16] a) L. Tuscher, C. Helling, C. Wölper, W. Frank, A. S. Nizovtsev, S. Schulz, *Chem. Eur. J.* **2018**, *24*, 3241–3250; b) J. Krüger, J. Schoening, C. Ganesamoorthy, L. John, C. Wölper, S. Schulz, *Z. Anorg. Allg. Chem.* **2018**, *644*, 1028–1033; c) L. Song, J. Schoening, C. Wölper, S. Schulz, P. R. Schreiner, *Organometallics* **2019**, *38*, 1640–1647.

[17] a) L. Tuscher, C. Ganesamoorthy, D. Bläser, C. Wölper, S. Schulz, *Angew. Chem. Int. Ed.* **2015**, *54*, 10657–10661; *Angew. Chem.* **2015**, *127*, 10803–10807; b) L. Tuscher, C. Helling, C. Ganesamoorthy, J. Krüger, C. Wölper, W. Frank, A. S. Nizovtsev, S. Schulz, *Chem. Eur. J.* **2017**, *23*, 12297–

Chemistry–A European Journal

Full Paper
doi.org/10.1002/chem.202001739

Chemistry
Europe
European Chemical
Societies Publishing

12304; c) J. Krüger, C. Wölper, S. Schulz, *Inorg. Chem.* **2020**, *59*, 11142–11151.

[18] a) J. Krüger, C. Ganesamoorthy, L. John, C. Wölper, S. Schulz, *Chem. Eur. J.* **2018**, *24*, 9157–9164; b) J. Schoening, L. John, C. Wölper, S. Schulz, *Dalton Trans.* **2019**, *48*, 17729–17734.

[19] J. Krüger, C. Wölper, L. John, L. Song, P. R. Schreiner, S. Schulz, *Eur. J. Inorg. Chem.* **2019**, 1669–1678.

[20] C. Ganesamoorthy, C. Helling, C. Wölper, W. Frank, E. Bill, G. E. Cutsail III, S. Schulz, *Nat. Commun.* **2018**, *9*, 87.

[21] a) P. P. Power, *Chem. Rev.* **2003**, *103*, 789–809; b) G. Tan, X. Wang, *Chin. J. Chem.* **2018**, *36*, 573–586; c) S. Ishida, F. Hirakawa, K. Furukawa, K. Yoza, T. Iwamoto, *Angew. Chem. Int. Ed.* **2014**, *53*, 11172–11176; *Angew. Chem.* **2014**, *126*, 11354–11358; d) R. Kretschmer, D. A. Ruiz, C. E. Moore, A. L. Rheingold, G. Bertrand, *Angew. Chem. Int. Ed.* **2014**, *53*, 8176–8179; *Angew. Chem.* **2014**, *126*, 8315–8318; e) T. Sasamori, E. Mieda, N. Nagahora, K. Sato, D. Shiomi, T. Takui, Y. Hosoi, Y. Furukawa, N. Takagi, S. Nagase, N. Tokitoh, *J. Am. Chem. Soc.* **2006**, *128*, 12582–12588; f) T. Li, H. Wei, Y. Fang, L. Wang, S. Chen, Z. Zhang, Y. Zhao, G. Tan, X. Wang, *Angew. Chem. Int. Ed.* **2017**, *56*, 632–636; *Angew. Chem.* **2017**, *129*, 647–651; g) S. Ishida, F. Hirakawa, T. Iwamoto, *Bull. Chem. Soc. Jap.* **2018**, *91*, 1168–1175.

[22] C. Helling, G. E. Cutsail III, H. Weinert, C. Wölper, S. Schulz, *Angew. Chem. Int. Ed.* **2020**, *59*, 7561–7568; *Angew. Chem.* **2020**, *132*, 7631–7638.

[23] C. Helling, C. Wölper, S. Schulz, *J. Am. Chem. Soc.* **2018**, *140*, 5053–5056.

[24] C. Helling, C. Wölper, Y. Schulte, G. Cutsail III, S. Schulz, *Inorg. Chem.* **2019**, *58*, 10323–10332.

[25] O. Coughlin, T. Krämer, S. L. Benjamin, *Dalton Trans.* **2020**, *49*, 1726–1730.

[26] H. Saleske, Ph.D. Dissertation, University of Würzburg, **1983**.

[27] P. Jutzi, K. Schwartzen, *Chem. Ber.* **1989**, *122*, 287–288.

[28] S. Singh, H.-J. Ahn, A. Stasch, V. Jancik, H. W. Roesky, A. Pal, M. Biadene, R. Herbst-Irmer, M. Noltemeyer, H.-G. Schmidt, *Inorg. Chem.* **2006**, *45*, 1853–1860.

[29] Crystallographic details are given in the electronic supplement.

[30] D. F. Evans, *J. Chem. Soc.* **1959**, 2003–2005.

[31] J. Weil, J. Bolton, *Electron Paramagnetic Resonance: Elementary. Theory and Practical Applications*, 2nd Ed., Wiley, Hoboken, New Jersey, **2007**.

[32] a) H. J. Breunig, M. Stanciu, R. Rösler, E. Lork, *Z. Allg. Anorg. Chem.* **1998**, *624*, 1965–1968; b) R. A. Baldwin, E. E. Foos, R. L. Wells, P. S. White, A. L. Rheingold, G. P. A. Yap, *Organometallics* **1996**, *15*, 5035–5038; c) A. Kuczkowski, S. Fahrenholz, S. Schulz, M. Nieger, *Organometallics* **2004**, *23*, 3615–3621; d) E. E. Foos, R. J. Jouet, R. L. Wells, P. S. White, *J. Organomet. Chem.* **2000**, *598*, 182–186; e) E. E. Foos, R. L. Wells, A. L. Rheingold, *J. Cluster Sci.* **1999**, *10*, 121–131; f) F. Thomas, S. Schulz, M. Nieger, *Z. Allg. Anorg. Chem.* **2002**, *628*, 235–242.

[33] J. C. Pando, E. A. Mintz, *Tetrahedron Lett.* **1989**, *30*, 4811–4812.

[34] M. Stubenhofer, C. Kuntz, M. Bodensteiner, A. Y. Timoshkin, M. Scheer, *Organometallics* **2013**, *32*, 3521–3528.

[35] M. Olaru, D. Duvinage, E. Lork, S. Mebs, J. Beckmann, *Angew. Chem. Int. Ed.* **2018**, *57*, 10080–10084; *Angew. Chem.* **2018**, *130*, 10237–10241.

[36] R. J. Schwamm, A. J. Edwards, C. M. Fitchett, M. P. Coles, *Dalton Trans.* **2019**, *48*, 2953–2958.

[37] C. Marquardt, O. Hegen, M. Hautmann, G. Balázs, M. Bodensteiner, A. V. Virovets, A. Y. Timoshkin, M. Scheer, *Angew. Chem. Int. Ed.* **2015**, *54*, 13122–13125; *Angew. Chem.* **2015**, *127*, 13315–13318.

[38] a) B. Miehlich, A. Savin, H. Stoll, H. Preuss, *Chem. Phys. Lett.* **1989**, *157*, 200–206; b) A. D. Becke, *Phys. Rev. A* **1988**, *38*, 3098–3100; c) C. Lee, W. Yang, R. G. Parr, *Phys. Rev. B* **1988**, *37*, 785–789.

[39] S. Grimme, S. Ehrlich, L. Goerigk, *J. Comput. Chem.* **2011**, *32*, 1456–1465.

[40] a) E. R. Davidson, A. E. Clark, *Int. J. Quantum Chem.* **2005**, *103*, 1–9; b) S. Fabig, G. Haberhauer, R. Gleiter, *J. Am. Chem. Soc.* **2015**, *137*, 1833–1843.

[41] L. Falivene, R. Credendino, A. Poater, A. Petta, L. Serra, R. Oliva, V. Scarano, L. Cavallo, *Organometallics* **2016**, *35*, 2286–2293.

[42] P. Jutzi, M. Kuhn, F. Herzog, *Chem. Ber.* **1975**, *108*, 2439–2447.